SYNERGISTIC USE OF OPTICAL AND INSAR DATA FOR URBAN IMPERVIOUS SURFACE MAPPING: A CASE STUDY IN HONG KONG

Liming Jiang[1,2]*, Hui Lin[1], Mingsheng Liao[2], Limin Yang[1,3]

[1]Institute of Space and Earth Information Science, Chinese University of Hong Kong, Shatin, N.T., Hong Kong, China
[2]State Key Laboratory of Information Engineering in Surveying, Mapping and Remote Sensing, Wuhan, China
[3]Raytheon Information Technology and Scientific Services (ITSS), EROS Data Center, U.S. Geological Survey, Sioux Falls, SD 57198, U.S.A.

KEY WORDS: Urban impervious surface, Classification and regression tree (CART); ERS-1/2 InSAR data; SPOT5 HRG imagery; Data fusion, Hong Kong

ABSTRACT:

A wide range of urban ecosystem studies, including urban hydrology, urban climate, land use planning and resource management require current and accurate geospatial data of urban impervious surfaces. In this study, the potential of the synergistic use of optical and InSAR data in urban impervious surface mapping was investigated. A case study in Hong Kong was conducted for this purpose by applying a CART-based ISP estimate approach to the SPOT 5 HRG imagery and the ERS-1/2 SLC SAR data. Validated by reference data derived from the high-resolution CIR aerial photographs, our results showed that the addition of InSAR feature information can improve the performance of SPOT-derived ISP estimation, average error (AE) value decreased from 15.51% to 12.93% and correlation coefficient (R2) value increased from 0.71 to 0.77.

1. INTRODUCTION

Impervious surfaces are usually defined as anthropogenic features through which water cannot infiltrate the soil, typically including buildings, roads, parking lots, sidewalks, and other built surfaces. Due to the close correlation with the spatial extent and intensity of urban development, impervious surface cover has been recently recognized as a key environmental indicator in assessing urban ecological condition and utilized to investigate urban hydrology, urban climate, land use planning, and resource management(Schueler 1994; Arnold and Gibbons 1996; Brabec 2002).

Over the past decade, extensive research efforts have been carried out to map impervious surfaces cost-effectively with satellite remote sensing data, especially multi-spectral optical images (e.g. Landsat TM/ETM+ or SPOT imagery). However, an accurate representation of impervious surface is still a challenge using these middle-resolution optical remote sensing data, because of the complexity of urban/suburban landscapes and the spectral confusions among different land-use/cover types (such as between barren land and parking lots)(Yang, Huang et al. 2003). The spectral confusion as well as the presence of mixed pixel may result in an overestimation of impervious surface distribution in the less-developed areas, but underestimation in the well-developed areas(Yang 2003; Wu 2004; Lu and Weng 2006). Unlike optical images that represent the spectral reflectivity of the targets illuminated by sun light, Synthetic Aperture Radar (SAR) images are very sensitive to the surface roughness, shape, structure, dielectric properties of the illuminated ground features and can provide information complementary to optical data(Henderson and Xia.Z 1997). In particular, several recent study progresses in radar remote sensing have demonstrated that the use of feature images (e.g. coherence, average intensity and intensity temporal change) derived from SAR interferometry (InSAR) pairs can improve the capability to distinguish natural features with man-made features(Bruzzone, Marconcini et al. 2004; Liao 2007).

The main aim of this study is to explore potentials of the synergistic use of optical and radar remote sensing data in mapping impervious surface cover. In particular, the CART-based approach was adopted to quantify urban impervious surfaces as a continuous variable (impervious surface percentage, ISP) by fusion of multi-sensor and multi-source datasets. The approach produces a rule-based model for prediction of ISP based on training data, and can allow impervious surface cover to be mapped at sub-pixel level of medium remote sensing data. A case study has been conducted for impervious surface mapping in Hong Kong by using the combined SPOT 5 HRG imagery and ERS-1/2 InSAR data. Results show that the fusion of the optical and InSAR data can significantly improve the performance of ISP estimation.

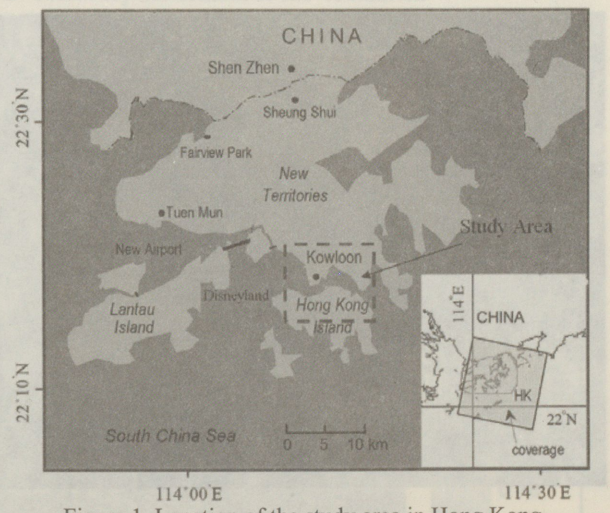

Figure 1. Location of the study area in Hong Kong

* Corresponding author: Liming Jiang. Email: JIANGLIMING@CUHK.EDU.HK

2. STUDY AREA AND DATA SET

2.1 Description of study area

The study area covers about 100 km^2 along both sides of the Victoria Harbor, Hong Kong and is located within latitude 22.267°N~22.343°N, longitude 114.122°E~114.240°E (Figure 1). It includes Kowloon and Hong Kong Island, which are both well-known central business districts (CBD). The study area consists of dense urban area, bared filed, mixed vegetation and open water. The urban areas along Victoria Harbour are even, but the bottom and upper left parts in the study area are rolling piedmont terrain covered with dense and mixed vegetation.

SAR sensor	Orbit number	Time	Time interval (day)	Spatial perp. baseline(m)
ERS-2	18795	1998-11-24	35	-13
ERS-2	19296	1998-12-29		

Table 1 the basic parameters of ERS SAR interferometric pairs in this study

2.2 Datasets and pre-processing

In this study, a pair of ERS-2 C-Band Single Look Complex (SLC) SAR data were chosen for generating feature images of interferometric SAR signature (Table 1). This InSAR pair was characterized with a short spatial perpendicular baseline (-13 m) and a relatively long-term interval (35 days). Unlike the Tandem coherence derived from ERS-1/2 images and used in standard approaches, a long-term coherence image computed from the considered InSAR pair can improve capacity to distinguish man-made features with other urban land-covers(Bruzzone, Marconcini et al. 2004; Liao 2007). This is due to the fact that coherence of man-made features remains high even between image pairs separated by a long time interval (months to years), however, most of natural land surfaces (e.g. farmland and forest field, etc.) are significantly influenced by temporal decorrelation and lose coherence within a few days. In addition, average amplitude and amplitude ratio were obtained from the same InSAR pair and an RGB combination of the three resulted feature images was shown in Figure 2(a).

In addition, a SPOT 5 HRG multi-spectral imagery acquired in November, 2002 was used in this study. The SPOT 5 image had three bands in visible and NIR bands (0.50-0.59 um, 0.61-0.68 um, 0.79-0.89 um) with 10 meter spatial resolution and one in SWIR band (1.58 – 1.75 um) with 20 meter resolution (Figure 2 (b)). In particular, a Colour-Infrared (CIR) aerial photography acquired in November, 2000 was utilized to derive training/test data for an ISP CART-based prediction model based and validation data for accuracy assessment of ISP mapping. The CIR aerial photograph was scanned color balanced into a digital format with 33-cm nominal spatial resolution. The SPOT 5 data and the CIR aerial photograph were geometrically corrected and ortho-rectified to Hong Kong 1980 Grid Map Projection using a 1:5, 000 Digital Elevation Model (DEM) data of Hong Kong.

For merging multi-sensors remote sensing data, several pre-processing steps are necessary to establish a more direct relationship between image signals and physical phenomena. In this study, some standard InSAR pre-processing steps were applied to the two ERS-2 SLC SAR data above, mainly including radiometric calibration, coregistration (with 0.1 pixel accuracy), a temporal SAR speckle filtering applying to amplitude images, and deviation of InSAR features (coherence, average amplitude and amplitude ratio). In order to geocode the InSAR products, the satellite precision orbit data and the mentioned large-scale DEM data were utilized to generate a geocoding lookup table for the conversion between DEM projection coordinate and SAR imaging geometry. The geocoding process was completed with sup-pixel accuracy by using GAMMA DIFF&GEO module (www.gamma-rs.ch). The geocoded InSAR products, coherence image, average amplitude image and amplitude ratio image, finally were resampled at 10 m spatial resolution as same as the SPOT data.

3. METHODOLOGY

In this case study, a CART-based approach developed by Yang (2003) was adopted to estimate sub-pixel percentage of impervious surface with the synergistic use of SPOT multi-spectral imagery and InSAR products. This approach used high-resolution imagery as a source of training data for representing urban land-cover heterogeneity, and medium-resolution imagery to extrapolate imperviousness over large spatial areas.

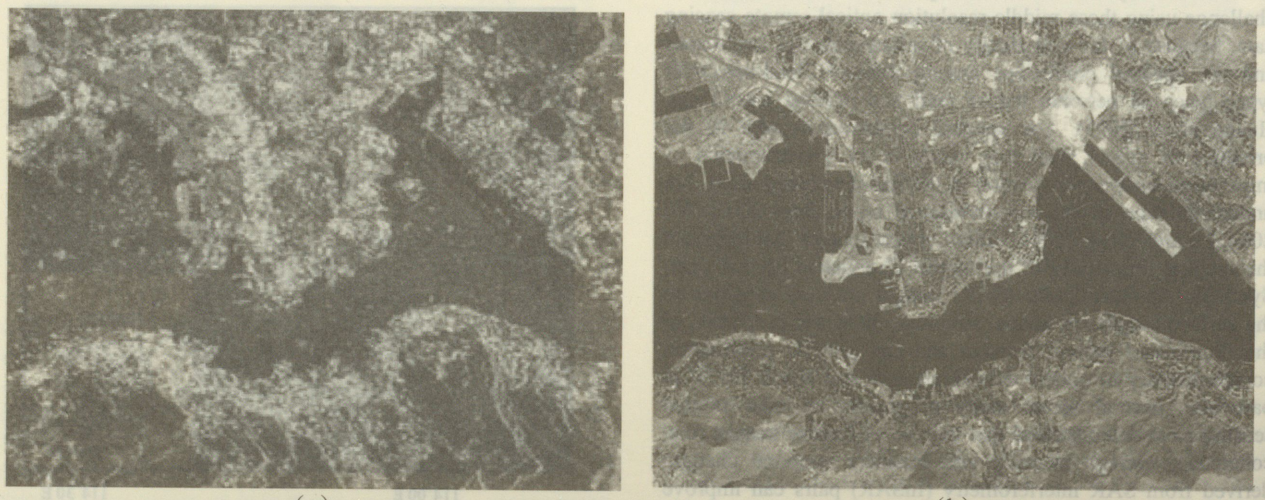

(a) (b)

Figure 2 The medium-resolution remote sensing data set in the study area (a)ERS-2 InSAR data (Red-Coherence, Green-Interferogram amplitude, Blue-Amplitude ratio); (b) SPOT5 HRG data(Red-Band4, Green-Band1, Blue-Band3,)

An advantage of this CART-based approach over other ISP estimation approaches based on spectral clustering (e.g., spectral mixture analysis) is their applicability to use multi-source and multi-sensor remote sensing data which are characterized with different statistical distribution and different physical feature. In addition, it permits the exploration of large-area impervious surface information at sup-pixel level in a repeatable and objective way. In this study, the process of mapping impervious surface using the CART-based approach involves the following steps (as shown in Figure 3): 1) development of training/test data using 33cm-resolution digital aerial CIR photography, 2) design of predictive variables, establishment and assessment of final regression tree modelling, 3) spatial extendibility of ISP prediction modelling with middle-resolution remote sensing dataset, and 4) accuracy assessment of ISP mapping.

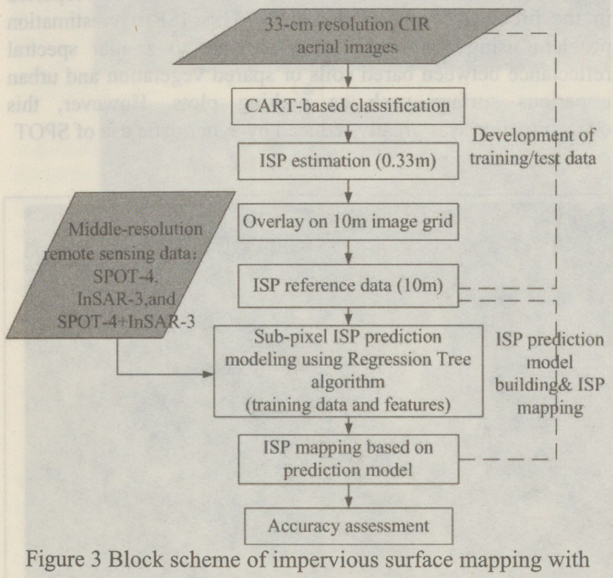

Figure 3 Block scheme of impervious surface mapping with remote sensing data and a regression tree model

3.1 Development of ISP training/test data

Successful ISP prediction modelling using CART algorithm relies on the quality of training-test data. In this study, training and test data were derived from four subset patches of the 33cm-resolution CIR aerial image. These image subsets were approximately 2000 x 1500 m each and were visually selected to avoid areas where land cover changes occurred among the CIR aerial images, the SPOT imagery and the InSAR products.

Initially, the selected CIR aerial images were classified using the CART machine learning algorithm. Each pixel was classified as one of five land cover classes: impervious surface, vegetated areas, bared soil, water, and shadow. The classifications were further modified by screen digitizing and recoding to reduce misclassification. Validated by the in situ data, the classification results archived overall accuracy 87.56% and Kappa coefficient 0.811. Once the final classification results were obtained, all 33-cm resolution pixels mapped as impervious surface were tallied using a 10 × 10 m grid geographically aligned with the middle-resolution data pixels (10m resolution corresponding to SPOT and InSAR data in this study) to compute percent impervious surfaces. This resulted in 10-m resolution raster image of percent imperviousness. It is noted that the shadow class was excluded from the calculation of imperviousness in this process since the class could not be unambiguously merged with any single land cover class. Figure5 illustrates one of the four CIR aerial image subsets and its ISP image with 10-m spatial resolution.

3.2 ISP prediction model building and ISP mapping

An ISP prediction model based on the CART regression tree algorithm was developed and calibrated by using the training/test data above obtained from high-resolution CIR aerial image as dependent variable (target variable). In addition, the independent variables (predictor variable) were derived from the six layer including three SPOT multi-spectral images and three InSAR feature images. In this study, 2000 training samples and 2000 testing samples were randomly selected from the layers of target and predictor variables. It is worth nothing that the training samples were independent to the test samples.

The training/test samples were utilized to build and improve the rule-based ISP prediction model by using the CART regression tree algorithm. The prediction model was composed of rule sets where each rule was defined by one or more conditions and corresponding confidence-level under which a multivariate linear regression model was established. Once the final ISP prediction model was built, it was applied to all pixels of the six middle-resolution remote sensing dataset to map percent impervious surfaces.

3.3 Accuracy assessment of ISP estimation

For accuracy assessment of ISP estimate, the reference data should ideally be collected from the field work based on a statistical sampling design. Due to time and resource constraints, the 10-m resolution ISP derived from the CIR aerial image was

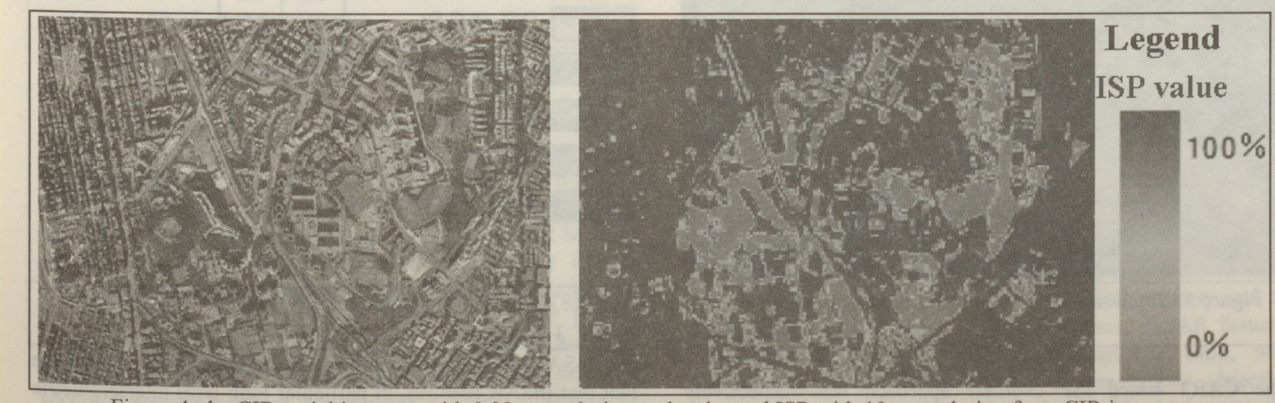

Figure 4 the CIR aerial imagery with 0.33m resolution and estimated ISP with 10m resolution from CIR imagery

used for this purpose. To ensure the validity of the assessment,

all the reference data were selected randomly and independently from the training/test data used in building ISP prediction model above.

In addition, the ISP map produced from the remote sensing dataset in this study belongs to continuous data. Therefore, the accuracy assessment method based on error matrix and kappa index used often in classification cannot be appropriate here because it is designed for categorical data only. In this study, correlation analysis was used for the quantitative comparison between the estimated ISP and the reference data. Three indicators, Average Error (AE), Relative Error (RE) and Pearson coefficient (R2), were calculated to assess accuracy of the ISP estimation.

4. EXPERIMENT RESULTS

To test the effectiveness and feasibility of the synergistic use of optical and InSAR data in urban ISP mapping, three group of data sources used in this study were (1) 4 SPOT HRG multi-spectral bands, here referred to SPOT_4, (2) 3 InSAR products (referred to InSAR_3), and (3) 4 SPOT bands plus 3 InSAR products (referred to SPOT_4+InSAR_3).

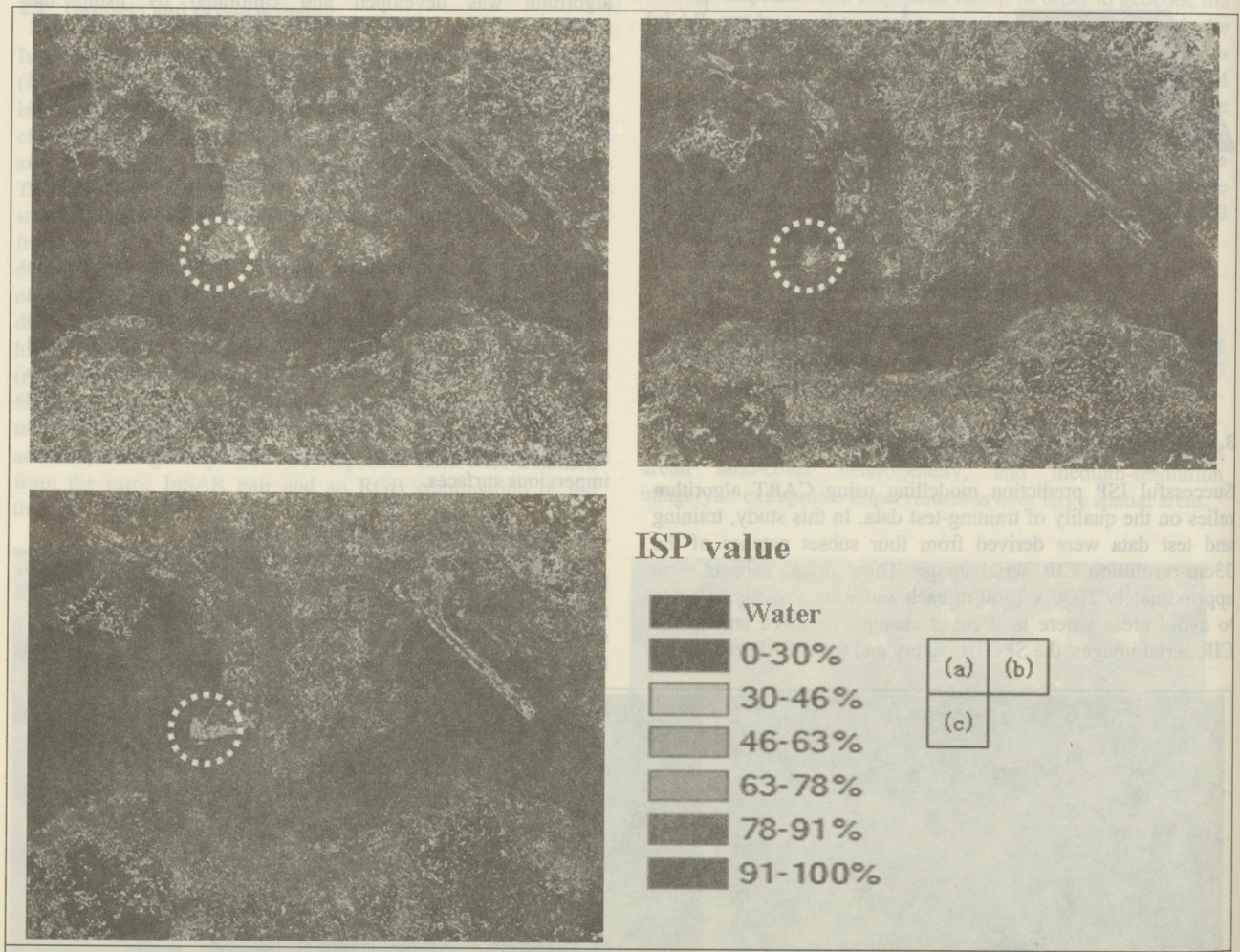

Figure 5 ISP classification results derived from the three groups of remote sensing datasets in the study area （a）InSAR_3; （b）SPOT_4; （c） InSAR_3+SPOT_4

The CART based ISP estimate approach was respectively applied to the three data sources and corresponding ISP prediction models were built. The classification results of ISP estimate derived from the three groups of middle-resolution remote sensing dataset were illustrated in Figure6. They were post-processed by masking sea water boundary. Figure6 shows that The ISP of the urban area located in the commercial business district of Kowloon and Hong Kong Island was greater than 60%, and that of the suburbs and hill areas was less than 40%.

Visually, three ISP results shown in Figure 6 were quite reasonable in spatial distribution pattern and the density urban areas with high ISP value were similarly mapped. But the ISP estimate results using just InSAR products were fragmentized due to coarse spatial resolution and signal distortion in roll areas (Figure 5(a)). In addition, checking by the use of high-resolution CIR aerial photographs suggested that the SPOT-derived ISP was slightly overestimated in the low to middle ISP areas (e.g., bared soils or vegetated fields) as has been reported in the previous works (Figure5(b)). This ISP overestimation problem using SPOT data may be due to similar spectral reflectance between bared soils or spared vegetation and urban imperious surface such as parking plots. However, this overestimation was greatly reduced by synergistic use of SPOT and InSAR dataset (Figure 5(c)). It should be attributed to the fact that InSAR features, in particular long-term interferometric coherence, possessed the capacity to distinguish the two land-cover classes mentioned above. It further and in detail was

demonstrated by the ISP results of the typical area selected in study area that located near the West Kowloon Waterfront Promenade and covered with bared soils and sparse grass. The spectral confusion resulted in a dramatically ISP overestimation in the mixed area using just SPOT imagery and ISP values were up to more than 78% (Figure 6(b)), but less than 60% after considering InSAR feature information (Figure 6 (c)).

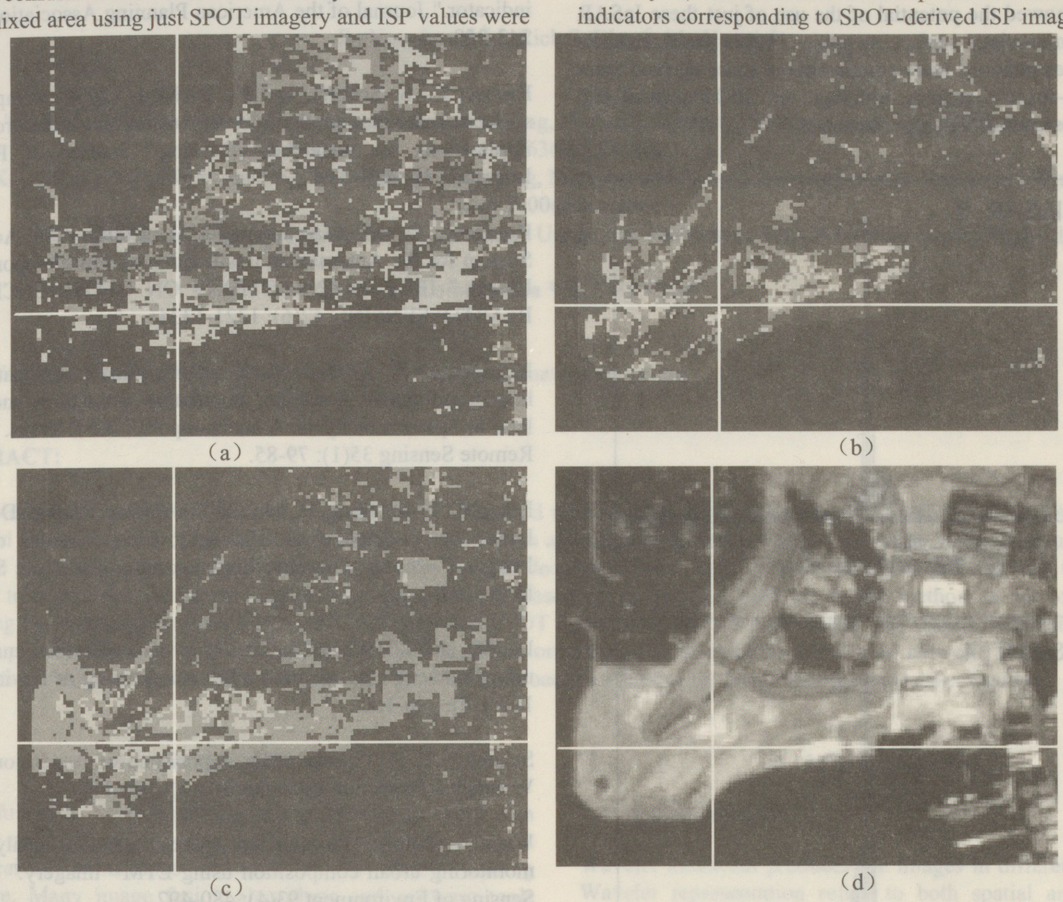

Figure 6 Comparison of ISP estimated results at reclamation region in Yau Ma Tei (a) InSAR_3; (b) SPOT_4; (c)SPOT_4+InSAR_3 ; (d)SPOT imagery

Dataset	Statistical indictor		
	Average error (*AE*) (%)	Relative Error (*RE*)	Pearson coefficient (R^2)
InSAR_3	19.27	0.69	0.61
SPOT_4	15.51	0.58	0.71
InSAR_3+SPOT_4	12.93	0.51	0.77

Table 2 accuracy assessment of ISP estimation results

In this study, a quantitative validation analysis was conducted for the accuracy assessment of ISP estimation results. Approximately 7252 samples were selected randomly independently from the reference data and ISP images that derived by using middle-resolution dataset. It should be noted that these samples did not include those used for the ISP prediction model development. The statistical indicators, Average Error (AE), Relative Error (RE) and Pearson coefficient (R2), were calculated for the three ISP images derived from the three groups of test datasets. The results of accuracy assessment were summarized in Table 2. The results indicated that InSAR-derived ISP estimations were comparable to those derived from SPOT multi-spectral images, although the SPOT-derived ISP images represented a higher performance (AE 15.51%, RE 0.58 and R2 0.71). As was expected, the addition of the InSAR feature information improved the accuracy of ISP estimate. Compared to these statistical indicators corresponding to SPOT-derived ISP image, AE value decreased by about 3 percent to 12.93% and R2 value increased from 0.71 to 0.77. In addition, the difference between the estimated ISP vales and reference data were calculated and demonstrated by the error histogram. Compared with the error histograms of InSAR-derived and SPOT-derived ISP estimate, the one of fused data represented an apparent peak near the zero value and more than 80% of the estimate error fell near the peak.

5. CONCLUSIONS

This study focused on urban impervious surface mapping by using the combined multi-sources and multi-sensors remote sensing dataset. Because of information complementarities between optical and radar imagery, we have demonstrated that the synergistic use of this two data sources has the potential to improve the ISP estimate performance, especially in some areas coved with bared soils or sparse vegetation.

In this paper, a case study was conducted for impervious surface mapping in Hong Kong by applying the CART-based ISP estimate approach to the SPOT 5 HRG imagery and the ERS-1/2 SLC SAR data. In particular, three InSAR features, coherence, average amplitude and amplitude ratio, were extracted from the SAR data for the investigate objective. Validated by reference data derived from the high-resolution CIR aerial photographs, our results show that the addition of

InSAR feature information can improve the performance of SPOT-derived ISP estimation, average error (AE) value decreased by about 3 percent to 12.93% and correlation coefficient (R2) value increased from 0.71 to 0.77. In addition, the results showed the potential of the use of just these InSAR features in impervious surface mapping. In this paper, InSAR-derived ISP estimations were comparable to those derived from SPOT multi-spectral images, although the SPOT-derived ISP images represented a higher performance.

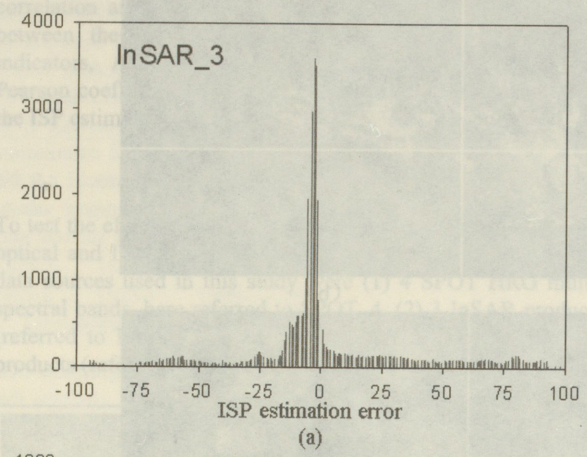

(a)

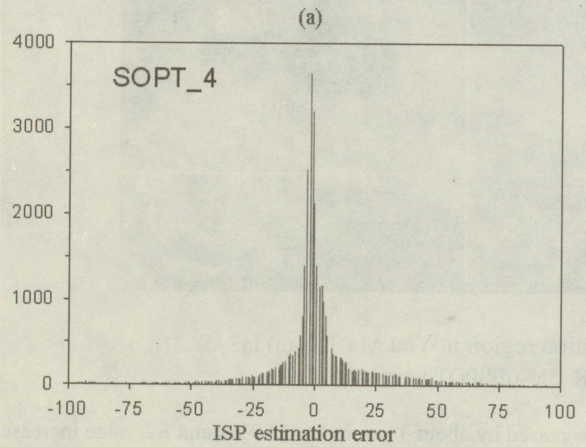

(b)

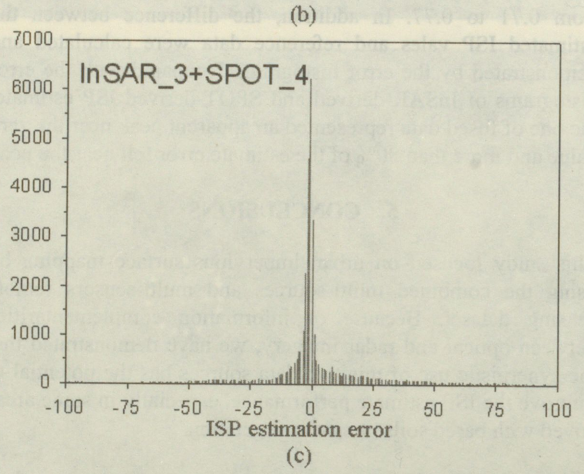

(c)

Figure 7 Error histogram of estimated ISP derived from 3 groups of remote sensing datasets （a）InSAR_3；（b）SPOT_4；（c）InSAR_3+SPOT_4

REFERENCE:

Arnold, J. C. A. and C. J. Gibbons (1996). "Impervious surface coverage: The emergence of a key urban environmental indicator." Journal of the American Planning Association 62(2): 243-258.

Brabec, E., S. Schulte, and PL Richards (2002). "Impervious surfaces and water quality: a review of current literature and its implications for watershed planning." Journal of Planning Literature 16: 499–514.

Bruzzone, L., M. Marconcini, et al. (2004). "An Advanced System for the Automatic Classification of Multitemporal SAR Images." IEEE TRANSACTIONS ON GEOSCIENCE AND REMOTE SENSING 42(6): 1321-1334.

Henderson, F. M. and Xia.Z (1997). "SAR applications in human settlement detection, population estimation and urban land use pattern analysis: A status report." IEEE Trans. Geosci. Remote Sensing 35(1): 79-85.

Liao, M., L. M. Jiang, H. Lin (2007). "Urban Change Detection Based on Coherence and Intensity Characteristics of SAR Imagery." Photogrammetric Engineering and Remote Sensing, In Press.

Lu, D. and Q. Weng (2006). "Use of impervious surface in urban land-use classification." Remote Sensing of Environment 102(1-2): 146-160.

Schueler, T. R. (1994). "The importance of imperviousness." Watershed Protection Techniques 1(3): 100-111.

Wu, C. (2004). "Normalized spectral mixture analysis for monitoring urban composition using ETM+ imagery." Remote Sensing of Environment 93(4): 480-492.

Yang, L., C. Huang, et al. (2003). "An approach for mapping large-area impervious surfaces: Synergistic use of Landsat 7 ETM+ and high spatial resolution imagery." Canadian Journal of Remote Sensing 29(2): 230-240.

Yang, L., Xian, G., Klaver, J. M., & Deal, B (2003). "Urban land-cover change detection through sub-pixel imperviousness mapping using remotely sensed data." Photogrammetric Engineering and Remote Sensing 69(9): 1003-1010.

ACKNOWLEDGEMENT

The work in this paper was supported by Competitive Earmarked Research Grant of the Hong Kong Research Grant Council (No. CUHK4665/06H) and Social Science and Education Panel Direct Grant of the Chinese University of Hong Kong. The first author was grateful to the Chinese University of Hong Kong for the Postgraduate Research Scholarship provided.